Predicting Accurate Electronic Excitation Transfer Rates via Marcus Theory with Boys or Edmiston−Ruedenberg Localized Diabatization†

Joseph E. Subotnik,*,‡,¶ Josh Vura-Weis,*,‡ Alex J. Sodt,§ and Mark A. Ratner‡

Department of Chemistry, Northwestern University, Evanston, Illinois 60208, and Laboratory of Computational Biology, National Heart, Lung, and Blood Institute, National Institutes of Health, Bethesda, Maryland 20892

Received: February 8, 2010; Revised Manuscript Received: April 7, 2010

We model the triplet−triplet energy-transfer experiments from the Closs group [Closs, G. L.; et al. *J. Am. Chem. Soc.* **1988**, *110*, 2652.] using a combination of Marcus theory and either Boys or Edmiston−Ruedenberg localized diabatization, and we show that relative and absolute rates of electronic excitation transfer may be computed successfully. For the case where both the donor and acceptor occupy equatorial positions on a rigid cyclohexane bridge, we find $\beta_{calc} = 2.8$ per C−C bond, compared with the experimental value $\beta_{exp} = 2.6$. This work highlights the power of using localized diabatization methods as a tool for modeling nonequilibrium processes.

1. Introduction: Modeling The Closs Experiments

Twenty years ago, in a series of elegant experiments, Closs and co-workers[1,2] measured the rates of electronic excitation transfer (EET) or electron transfer (ET) from either benzophenone or biphenyl to naphthalene across a variety of bridge molecules at room temperature. Several conclusions were immediately clear from their results. First, for a rigid bridge molecule, the rate of triplet EET decayed exponentially with the number of bridging covalent bonds, consistent with the superexchange mechanism. Second, the rate of triplet EET was roughly proportional to the rate of electron transfer times the rate of hole transfer (with a properly dimensioned coefficient to account for solvation and reorganization). Thus, the Closs experiments reinforced the idea that ET and EET could and should be considered within the same theoretical framework.

In this article, we will computationally model the Closs EET experiments, and we will show that experimental EET rates may be successfully calculated when we combine Marcus theory[3,4] with straightforward techniques from ab initio electronic structure theory. These techniques might be labeled localized diabatization, and they are very similar to orbital localization techniques from quantum chemistry.[5] Intriguingly, these methods can be applied to both ET and EET equivalently; in a future paper, we will calculate the corresponding ET results and compare them with experimental values. Computational studies of ET in cyclohexane-bridged systems have been reported previously by Braga and Larsson[6] and Koga, Sameshima, and Morokuma.[7] The latter work also addresses EET partially.

An outline of this paper is as follows. In section 2, we will present the necessary theoretical background for modeling EET in terms of Marcus theory for real, three-dimensional chemical systems and discuss localized diabatization. In section 3, we present numerical results for the range of bridge molecules considered by Closs and co-workers. In section 4, we discuss our findings before concluding in section 5.

2. Theory

2.1. Marcus Theory Applied to Electronic Excitation Transfer (EET). According to Marcus theory, in the nonadiabatic high-temperature or activated crossing limit, the rate of EET in a condensed environment is[8,9]

$$k_{I\to F} = \frac{2\pi}{\hbar}|H_{IF}|^2\sqrt{\frac{1}{4\pi k_B T\lambda}}e^{-(\lambda + \Delta G^0)^2/4\lambda k_B T} \qquad (1)$$

Here, "I" represents the initial state of the system, "F" represents the final state of the system, and H_{IF} is the diabatic electronic coupling matrix element between the two electronic states. ΔG^0 is the total change in free energy between the final and initial states ($E_F - E_I$, ignoring entropy changes), and λ is the reorganization energy, which accounts for the motion of solvent and other nuclei. Equation 1 is valid in both the Dexter[10] and Forster[11,12] limits of EET, but as we will see, the experiments here are in the Dexter regime.

In order to derive eq 1, several assumptions have been made. First, one assumes that the potential energy surfaces for the nuclear vibrational modes are two shifted parabolas. Second, one assumes the validity of the golden rule or first-order time-dependent perturbation theory. Third and finally, we take the high-temperature or activated crossing limit, $k_B T \gg (\hbar\omega)^2/\lambda$, where ω is the maximum frequency for any nuclear vibrational mode coupled to the electronic system.[8,9,13] This last assumption is usually not valid for EET events, as discussed in section 3.3. As a practical matter, standard Marcus theory can be derived easily if one assumes that all nuclear coordinates may be grouped together into one effective reaction coordinate. In this case, ω is chosen to be the frequency of that reaction coordinate, and eq 1 follows from transition-state theory.[8] More elaborate versions of Marcus theory exist.[14]

Given the above assumptions, it is clear that the Marcus equation applies rigorously only for a model Hamiltonian. For a real system that can be experimentally probed, the necessary assumptions can be only approximately true. As a result, even

† Part of the "Klaus Ruedenberg Festschrift".

* To whom correspondence should be addressed. E-mail: subotnik@sas.upenn.edu (J.E.S.); vura-weis@northwestern.edu (J.V.-W.).

‡ Northwestern University.

§ National Institutes of Health.

¶ Present Address: Department of Chemistry, University of Pennsylvania; as of July, 2010.

10.1021/jp101235a
Published on Web 05/06/2010

if we are willing to assume that the golden rule applies, three new problems arise for practical predictions of EET rates:

(1) Starting with rigorous ab initio calculations of adiabatic electronic states $|\Phi_1\rangle$,$|\Phi_2\rangle$, how do we define the diabatic states $|\Xi_I\rangle$,$|\Xi_F\rangle$ that represent the initial and final states of the EET process? Intuitively, for the initial state, the electronic excitation should be localized on the donor, and for the final state, the electronic excitation should be on the acceptor, $|\Xi_I\rangle = |AD^*\rangle$ and $|\Xi_F\rangle = |A^*D\rangle$. How can such states be constructed for intramolecular EET where, in general, the adiabatic states $|\Phi_1\rangle$,$|\Phi_2\rangle$ are mixtures of the initial and final states $|\Xi_I\rangle$,$|\Xi_F\rangle$?

(2) For physical problems, the potential energy surfaces will not be parabolas, and the diabatic coupling H_{IF} will not be constant. By definition, a varying H_{IF} is a violation of the so-called Condon approximation. Thus, at what geometry should we calculate H_{IF} in order to best match experiment?[8]

(3) Because calculations are most easily done in vacuum, how can we best and most easily approximate the reorganization energy?

In this paper, we will solve the first problem by constructing diabatic states using localized diabatization algorithms, in particular the Boys and Edmiston−Ruedenberg (ER) formalisms. As described in detail previously[5,15] and briefly below, these diabatic states arise when one assumes that there are external electrostatic interactions stabilizing the localization of either charge or energy excitation.

For the second problem, we will test the Condon approximation by choosing different molecular geometries and comparing the resulting different values of H_{IF}. According to the Condon approximation, over regions of nuclear configuration space where the electronic energies of adiabatic states do not change significantly, the electronic coupling H_{IF} should be constant. Our general conclusion will be that, for rigid bridge molecules, the Condon approximation is nearly satisfied. For small and flexible bridge molecules, especially when torsional angles are not fixed, the Condon approximation can be badly violated, and standard Marcus theory may be inapplicable or need correction. This conclusion agrees with previous ET results.[7]

Finally, regarding the reorganization energy, we note that because charge is never displaced from one basin to another, we expect that reorganization energies should be relatively constant for EET. More generally, we will calculate optimized nuclear geometries corresponding to electronic configurations $|AD^*\rangle$ and $|A^*D\rangle$ by biasing the initial guess geometry and then minimizing the energy. Using the resulting optimized geometries, we can calculate precise reorganization energies and energy shifts. We will find that reorganization energies are not important for modeling the relative EET rates in the Closs experiments. If, however, we do calculate the reorganization energies, absolute EET rates may also be calculated with some success.

2.2. Brief Review of Localized Diabatization and the Diabatic Coupling H_{IF}. Before applying Marcus theory to the EET experiments of Closs and co-workers, we briefly review how localized diabatization is implemented for a real chemical system. This is how we solve problem (1) above.

2.2.1. Boys and ER Diabatization. By definition, for any problem in quantum mechanics, the adiabatic states of a system $|\Phi_j\rangle$ are those electronic states that diagonalize the electronic Hamiltonian, assuming that the nuclei are fixed

$$H(r,R) = H_{nuc}(R) + H_{el}(r;R) \tag{2}$$

$$H_{el}(r;R)|\Phi_j(r;R)\rangle = E_j(R)|\Phi_j(r;R)\rangle \tag{3}$$

In eqs 2 and 3, r represents electronic coordinates, and R represents nuclear coordinates.

When external degrees of freedom are present (either from a bath of solvent or from nuclear vibrations), the adiabatic states of the system may not be stationary. Moreover, the adiabatic states may not represent the initial or final states of an ET or EET process. In such cases, one standard approach to describe the electronic stationary states of the system is to rotate the adiabatic states into a set of diabatic states $\{|\Xi_i\rangle\}$

$$|\Xi_i\rangle = \sum_{j=1}^{N_{states}} |\Phi_j\rangle U_{ji} \qquad i = 1...N_{states} \tag{4}$$

Several techniques have been previously introduced for generating the rotation matrix $\mathbf{U}$ using a variety of different approaches. Early techniques searched for the crossing seam[16,17] where

$$\mathbf{U} = \frac{1}{\sqrt{2}}\begin{pmatrix} 1 & -1 \\ 1 & 1 \end{pmatrix}$$

and then used a splitting criterion to calculate the diabatic coupling. This technique effectively localizes an electron on the donor and acceptor,[18] which can be seen most easily when one freezes all but one electron. More recently, a new group of methods have allowed diabatic couplings to be calculated at arbitrary nuclear geometries. Examples of such methods in the context of electron transfer include generalized Mulliken Hush (GMH)[19,20] and fragment charge difference (FCD),[21] and in the context of energy transfer, fragment energy difference (FED).[22–24]

We have previously argued that, on the basis of different models of system−bath coupling, one correct prescription for constructing such diabatic states is to use Boys, Edmiston−Ruedenberg (ER), or von Niessen−Edmiston−Ruedenberg (VNER) localization.[5,15] These three techniques make different assumptions about system−solvent interactions that all lead to localization of some kind.[5]

•Boys diabatization presumes that the bath exerts a linear electrostatic potential on the system.

•ER diabatization presumes that the bath exerts an electrostatic potential that responds linearly to the field of the system.

•Like ER diabatization, VNER diabatization presumes that the bath exerts an electrostatic potential that responds linearly to the field of the system, only with the extra stipulation that system charges and bound charges interact via a delta function potential (rather than by Coulomb's law).

As a practical matter, the assumptions above lead to rotation matrices $\mathbf{U}$ characterized by maximizing three different localizing functions[5]

$$f_{Boys}(\mathbf{U}) = f_{Boys}(\{\Xi_i\}) = \sum_{i,j=1}^{N_{states}} |\langle\Xi_i|\vec{\mu}|\Xi_i\rangle - \langle\Xi_j|\vec{\mu}|\Xi_j\rangle|^2 \tag{5}$$

$$f_{\mathrm{ER}}(\mathbf{U}) = f_{\mathrm{ER}}(\{\Xi_i\}) = \sum_{i=1}^{N_{\mathrm{states}}} \int \mathrm{d}\underline{\mathbf{r}}_1 \int \mathrm{d}\underline{\mathbf{r}}_2 \frac{\langle \Xi_i|\hat{\rho}(\underline{\mathbf{r}}_2)|\Xi_i\rangle\langle \Xi_i|\hat{\rho}(\underline{\mathbf{r}}_1)|\Xi_i\rangle}{|\underline{\mathbf{r}}_1 - \underline{\mathbf{r}}_2|} \quad (6)$$

$$f_{\mathrm{VNER}}(\mathbf{U}) = f_{\mathrm{VNER}}(\{\Xi_i\}) = -\sum_{i=1}^{N_{\mathrm{states}}} \int \mathrm{d}\underline{\mathbf{r}}(\langle \Xi_i|\hat{\rho}^2(\underline{\mathbf{r}})|\Xi_i\rangle - \langle \Xi_i|\hat{\rho}(\underline{\mathbf{r}})|\Xi_i\rangle^2) \quad (7)$$

where the density operator at position $\underline{\mathbf{r}}$ is defined to be $\hat{\rho}(\underline{\mathbf{r}})$

$$\hat{\rho}(\underline{\mathbf{r}}) = \sum_{j=1}^{\text{All Electrons}} \delta(\underline{\mathbf{r}} - \vec{r}_{(j)}) \quad (8)$$

and $\vec{r}_{(j)}$ is the position of the j^{th} electron. From the form of eqs 5 −7, it is clear that these diabatization algorithms correspond exactly to the localization routines that are standard tools in quantum chemistry for generating localized orbitals.[25–31]

Note that because the Boys algorithm separates charge according to eq 5, it is applicable only to ET and not to EET (since charge never separates in EET). As such, the ER algorithm is more powerful than the Boys approach for it describes both ET and EET equivalently. Nevertheless, in order to produce and compare two independent localization algorithms for EET, in this paper, we have implemented both ER diabatization and a modified Boys algorithm that is applicable to EET for CIS or TD-DFT adiabatic states. To generate this modified Boys method, we localize separately the electronic excitation and de-excitations of the excited states relative to the ground state. More concretely, we maximize the occupied−virtual separated Boys function (BoysOV) by separating the dipole operator into occupied and virtual components, $\mu = \mu^{\mathrm{occ}} + \mu^{\mathrm{virt}}$

$$f_{\mathrm{BoysOV}}(\mathbf{U}) = f_{\mathrm{BoysOV}}(\{\Xi_i\}) = \sum_{i,j=1}^{N_{\mathrm{states}}} |\langle \Xi_i|\vec{\mu}^{\mathrm{occ}}|\Xi_i\rangle - \langle \Xi_j|\vec{\mu}^{\mathrm{occ}}|\Xi_j\rangle|^2 + |\langle \Xi_i|\vec{\mu}^{\mathrm{virt}}|\Xi_i\rangle - \langle \Xi_j|\vec{\mu}^{\mathrm{virt}}|\Xi_j\rangle|^2 \quad (9)$$

All of the mathematical details behind eq 9 are given in the Appendix, section 1. Note that the decomposition $\mu = \mu^{\mathrm{occ}} + \mu^{\mathrm{virt}}$ works only for CIS or TD-DFT excited states.

Physically, according to eq 9, one assumes that holes and electrons may encounter different electrostatic fields; this assumption is not particularly reasonable, but because the final goal is primarily to produce diabatic states with localized electronic excitation, this algorithm may be sufficient. Furthermore, we can and will compare this algorithm versus rigorous ER localization for confirmation of its validity. Because an algorithm for implementing ER diabatization has already been published,[5] we provide only a few additional computational details needed for large molecules in section 2 of the Appendix.

2.2.2. Diabatic Coupling H_{IF}. Once the diabatic states of the system are known, the diabatic coupling that appears in eq 1 can be computed easily by changing representation. More specifically, if we have n electronic states, let the adiabatic energies be denoted ε_i ($i = 1, ..., n$), and let the adiabatic states be denoted $|\Phi_i\rangle$, so that

$$\langle \Phi_i|H^{\mathrm{el}}|\Phi_j\rangle = \delta_{ij}\varepsilon_i \quad (10)$$

When the diabatic states ($|\Xi_i\rangle$) are defined by the transformation $\mathbf{U}$ in eq 4, the diabatic couplings are simply the off-diagonal terms in the transformed Hamiltonian

$$\langle \Xi_i|H^{\mathrm{el}}|\Xi_j\rangle = \sum_{kl} U_{ki}\langle \Phi_k|H^{\mathrm{el}}|\Phi_l\rangle U_{lj} \quad (11)$$

For the two-state problem, with initial state I and final state F, the mathematical transformation can be written explicitly. Let $\mathbf{U}$ be parametrized by a mixing angle θ

$$\mathbf{U} = \begin{pmatrix} \cos(\theta) & -\sin(\theta) \\ \sin(\theta) & \cos(\theta) \end{pmatrix} \quad (12)$$

Now, if we transform to the diabatic representation, the Hamiltonian becomes

$$H^{\mathrm{el}} = \begin{pmatrix} \cos(\theta) & \sin(\theta) \\ -\sin(\theta) & \cos(\theta) \end{pmatrix}\begin{pmatrix} \varepsilon_1 & 0 \\ 0 & \varepsilon_2 \end{pmatrix}\begin{pmatrix} \cos(\theta) & -\sin(\theta) \\ \sin(\theta) & \cos(\theta) \end{pmatrix} \quad (13)$$

and the off-diagonal element H_{IF} is

$$H_{\mathrm{IF}} \overset{\mathrm{def}}{=} \langle \Xi_{\mathrm{I}}|H^{\mathrm{el}}|\Xi_{\mathrm{F}}\rangle = \frac{1}{2}\sin(2\theta)(\varepsilon_2 - \varepsilon_1) \quad (14)$$

Thus, solving for the adiabatic-to-diabatic transformation matrix $\mathbf{U}$ automatically yields a value for H_{IF} to be used in the context of Marcus theory.

In the next section, we will provide H_{IF} values (and mixing angles θ) for the Closs experiments. We will show that they match up very well with experimental EET rates.

3. Numerical Results: The Closs Experiments

The experimental results found by Closs and co-workers are listed in Table 1 along with our calculated H_{IF} values. Note that for these experiments, the EET occurred between triplet states; the triplet EET donor was benzophenone, and the triplet EET acceptor was naphthalene. In our work, for simplicity, we have substituted benzaldehyde for benzophenone; see Figure 1.

The H_{IF} values in Table 1 were generated according to the theory presented above. More specifically, the following steps were implemented using the ab initio quantum chemistry package Q-Chem:[32]

(1) For a fixed donor−bridge−acceptor geometry of the system, the Hartree−Fock (HF) orbitals for the singlet ground state were computed.

(2) A CIS triplet calculation was performed to find the lowest two adiabatic excited triplet states, T_1 and T_2. These states were easily shown to have $\pi \rightarrow \pi^*$ character.

(3) The two low-lying adiabatic triplet states were rotated together using either ER (eq 6) or BoysOV (eq 9) diabatization to generate the mixing angle θ and H_{IF} (eq 14).

(4) In order to be assured of meaningful results, the steps above were repeated while increasing the threshold for CIS convergence. A converged H_{IF} required a CIS relative error (in diagonalization) sometimes as small as 10^{-8}, mostly when the mixing angle θ was very small.

TABLE 1: H_{IF} Values for Donor (D)−Bridge−Acceptor (A) Systems with the Bridges Listed in Columns 1 and 2[a]

Symbol	Compound	k_{TT}^{ex} [1,2] (1/s)	$\|\theta\|$ (rad)	$\|H_{IF}\|$ (meV)	$\|H_{IF}\|$ (meV)	$\|H_{IF}\|$ (meV)	$\|H_{IF}\|$ (meV)	$\|H_{IF}\|$ (meV)
Diabatization Algorithm			ER	ER	BoysOV	BoysOV	BoysOV	BoysOV
Geometry optimized			Ground State	Ground State	Ground State	Ground State	T_1 A^*D	T_1 AD^*
Basis			6-31G**	6-31G**	6-31G**	cc-pVTZ	6-31G**	6-31G**
D-2,6ee	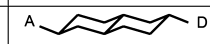	3.1×10^6	3.9×10^{-5}	0.020	0.020	0.019	0.020	0.022
D-2,7ee		9.1×10^7	3.3×10^{-4}	0.17	0.17	0.16	0.17	0.18
C-1,4ee	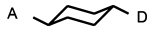	1.3×10^9	1.1×10^{-3}	0.56	0.56	0.57	0.61	0.60
C-1,3ee	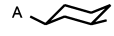	7.7×10^9	3.2×10^{-3}	1.5	1.5	1.4	1.6	1.6
D-2,6ae		1.3×10^5	2.2×10^{-6}	0.0010	0.0011	0.0011	0.0013	0.0017
D-2,6ea	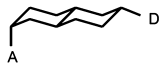	7×10^5	4.4×10^{-6}	0.0022	0.0019	0.0019	$< 0.0001^*$	0.0024
D-2,7ae		1.1×10^7	1.0×10^{-4}	0.049	0.052	0.053	0.058	0.054
D-2,7ea		1.5×10^7	1.0×10^{-4}	0.047	0.045	0.045	0.032	0.050
C-1,4ea	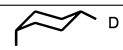	4×10^7	5.2×10^{-5}	0.026	0.034	0.037	0.066	0.043
C-1,3ea		3.3×10^9	9.4×10^{-4}	0.51	0.53	0.56	0.66	0.63
M	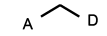	5×10^{10}	1.2×10^{-3}	0.56	0.64	0.79	6.0	0.31

[a] This infinitesimal coupling element designated with * is difficult to converge as the CIS error decreases; as such, here, we can only estimate an upper bound from our data.

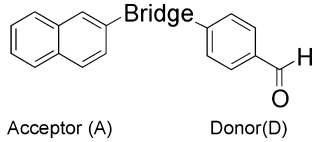

Figure 1. The donor (benzaldehyde) and acceptor (napthalene) fragments that are treated computationally in this article.

(5) In order to check the Condon approximation, the nuclear geometry of the system was changed, and the steps above were repeated. We also verified that our results did not depend on basis set.

Before analyzing the physical meaning of the numbers in Table 1, we note that in all calculations for this paper, the ER and BoysOV algorithms gave nearly identical diabatic couplings; the differences are usually well within 10%. For this reason, often, we will present only results from the BoysOV algorithm.

3.1. Choice of Geometry. Before calculating an H_{IF} value, the obvious question is: at what geometry should we be calculating it? According to the Condon approximation, the value of H_{IF} should be independent of geometry, but is this true in practice?

In Table 1, we check the Condon approximation by listing H_{IF} values at three different geometries, (i) the singlet ground-state geometry, (ii) the T_1 (first excited triplet state)-optimized geometry where the excitation is on the acceptor A*D, and (iii) the T_1 optimized geometry where the excitation is on the donor AD*. We note that, in almost all cases, our computed H_{IF} values depend very weakly on the geometry of the molecule. This is true for all of the equatorial−equatorial-substituted molecules and for most of the equatorial−axial-substituted ones. The most extraordinary exception to this rule is the case where the bridge is a flexible CH_2 group; in this case, H_{IF} changes dramatically, which is a violation of the Condon approximation, which will be discussed in section 4.2. For all other structures, there are rigid cyclohexane bridges between D and A, and we find that the Condon approximation is pretty good near the basin of the ground-state geometry.

Thus, for the moment, we are satisfied that we may predict EET rates (using eq 1) that will not depend strongly on molecular geometry within restricted geometric neighborhoods.

3.2. Relative EET Rates with Different Bridge Molecules. Going beyond the Condon approximation, by comparing the experimental and computational data in Table 1, we see that the experimental rate of triplet−triplet energy transfer is highly correlated with our computational value of H_{IF}. In order to make this correlation as clear as possible, in Figures 2 and 4, we plot the logarithm of the experimental EET rate versus the H_{IF} value. We do this separately for the case where (i) D/A are both equatorial or (ii) D/A are a combination of equatorial/axial.

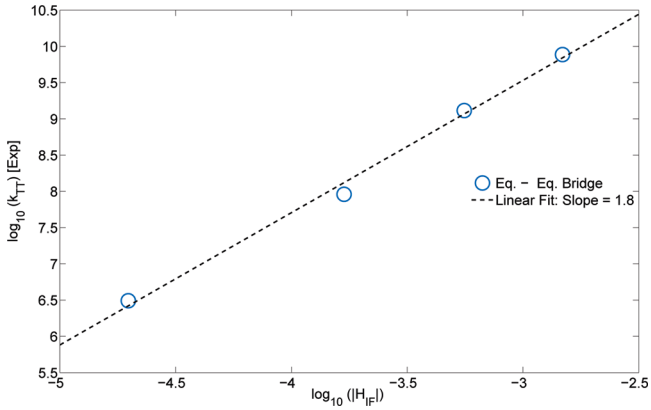

Figure 2. In blue, we plot log($|H_{IF}|$) versus the experimental rate constant log(k_{TT}^{exp}) for triplet−triplet energy transfer when D and A both occupy equatorial positions on cyclohexane. A line fit is also drawn in dotted black with a slope close to 2, showing that the reorganization energy must be nearly constant for this group of molecules. All diabatic couplings are computed at the singlet ground-state geometry with BoysOV localization and basis 6-31G**.

For the equatorial−equatorial data (Figure 2), note that the experimental and theoretical numbers are well fitted using linear interpolation with a slope of 1.8. Here, we plot H_{IF} values at the singlet ground-state geometry. Because the linear fit is so good and the slope is close to 2 (which corresponds to $|H_{IF}|^2$), it follows from this data that the golden rule (and time-dependent perturbation theory) applies to the relative rate of EET, and the reorganization energy is nearly constant across the different bridge molecules. As a confirmation of this claim, in Figure 3, we plot both the logarithm of the experimental rate constants and H_{IF}^2 versus the number of C−C bonds between the donor and acceptor. The curves are striking; we predict that the rate of transfer falls off exponentially (as in Dexter transfer) with $\beta_{calc} \approx 2.8$ per C−C bond compared to the experimental value of $\beta_{exp} \approx 2.6$. Note also that, in the next section, we will show that reorganization energies are indeed constant for these molecules. From all of this information, we conclude that computing H_{IF} with localized diabatization can be a powerful approach for predicting EET rates.

For the equatorial-axial data in Figure 4, the data points are not so obviously linear, and the resulting fitted curve is slightly less satisfying as the fitted line has a slope of 1.5 (rather than 2). As before, we plot H_{IF} values at the singlet ground-state geometry. In the next section, we show that reorganization energies are roughly constant for this series of molecules; therefore, the exponential prefactor in eq 1 cannot explain the slope of experiment versus theory. In this case, deviations from standard Marcus theory could be due to either of the following: (i) the potential energy surfaces for the nuclear coordinates may not be shifted parabolas, or (ii) the Condon approximation is not totally satisfied, and small changes in H_{IF} are important. From Table 1, we see that H_{IF} is indeed less constant for these molecules than that for the equatorial−equatorial molecules. In particular, for C-1,4ea, the value of $|H_{IF}|$ can change by more than a factor of 2 depending on the geometry, and the relative ordering of C-1,4ea and D-2,7ea can change. Nevertheless, without many more static and dynamical calculations, it is impossible to know how much deviation from Marcus theory comes from each of the above explanations. Nevertheless, the plot of experimental versus computational data does appear linear "enough", especially when one considers that the three points clustered around $k_{TT}^{exp} \approx 10^7$ s^{-1} have such similar experimental rate constants. Moreover, although the slope is not quite correct, 1.5 is not so far from 2, suggesting that some variation of a Marcus- or golden-rule-based formula must be roughly applicable.

Overall, the data in Table 1 predict that for rigid bridges, relative EET rates may be computed rather successfully using elementary excited-state theory (CIS) and localizing diabatization routines (i.e., BoysOV or ER localization). This is an encouraging development. In the next section, we will treat the question of how the prefactor multiplying H_{IF}^2 in eq 1 may be computed, so that absolute EET rates may be predicted as well.

3.3. Reorganization Energies and Absolute EET Rates. The final issue to be addressed in this paper is the reorganization energy that enters the prefactor multiplying H_{IF}^2 in eq 1. In the previous section, all geometric (or Franck−Condon) factors were ignored, and it was assumed that all reorganization and free energies were constant for the different donor−bridge−acceptor molecules. We now demonstrate numerically that this is really so. Furthermore, using eq 1, we show that the activated crossing limit of Marcus theory predicts absolute rates for EET that are close to experiment.

Starting with molecular geometries distorted toward either putative A*D or AD* electronic states, we optimized the geometry of each molecule in the first excited triplet state (denoted T_1) at the level of CIS triplets in a 6-31G** basis. We assumed that optimized adiabatic geometries should be close to the optimized diabatic geometries. All optimizations converged successfully to local minima, and thus, we found two different stable geometries for each molecule. These optimized structures are easily interpreted in terms of the Marcus parabolas; see Figure 5. Numerical results for ΔG^0 and λ are given in Table 2. For all molecules, we calculate λ in the range of $\lambda \in [0.8, 0.9]$ eV and ΔG^0 in the range of $\Delta G^0 \in [-0.55, -0.65]$ eV. From this data, for the case of a rigid bridge, the prefactor in eq 1 that multiplies H_{IF}^2 is between 0.8 and 1.2 $\times$ 10^{16}/(eV)^2/s and does not play a major role in explaining the relative rates.

In Table 3, we list absolute EET reaction rates according to eq 1. For the equatorial−equatorial molecules, our theoretical rates are roughly 2−4 times larger than experimental rates. The rates are about as accurate for the equatorial−axial molecules, with the exceptions of D-2,6ae and D-2,6ea. The reorganization energies and energy shifts for benzophenone and benzaldehyde are well within 0.1 eV of each other, and this substitution should not lead to significant changes in these predicted rates.

Overall, the high-temperature or activated crossing limit of Marcus theory (eq 1) mostly succeeds in calculating absolute EET rates for these molecules. This success comes despite several shortcomings of our own computational model. First, in our calculations, we have ignored the benzene solvent entirely. Second, by invoking standard Marcus theory, we assume that all of the nuclear vibrational modes are linearly coupled to the electronic system, so that the potential energy surfaces for the nuclei are shifted parabolas, which may not be true, especially for the equatorial−axial case. Third, the form of eq 1 is strictly applicable only in the high-temperature limit, when $k_B T \gg (\hbar\omega)^2/\lambda$,[8,9,13] where ω is a vibrational frequency. This statement is not usually true for most EET reactions, likely including our own. For $\lambda = 0.82$ eV and $T = 300$ K, assuming that there is one effective reaction coordinate, this requires that the frequency of that nuclear coordinate satisfy $\omega \ll 1150$ cm^{-1}.

In the future, it will be interesting to more fully investigate the dynamics of the EET process, quantifying the important nuclear modes coupled to the nonadiabatic event and estimating the error present when using eq 1 instead of the most general electron−phonon treatment.[8,9] In so doing, we may also learn

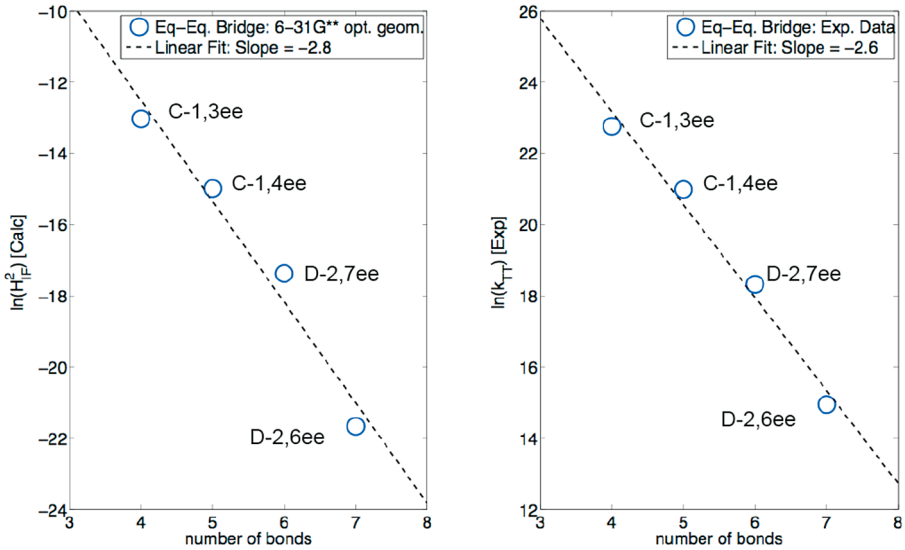

Figure 3. On the right-hand side, the logarithm of the experimental rate constant is plotted relative to the number of C−C bonds between the donor and acceptor ($\equiv n_b$), where both of the latter groups occupy equatorial positions. On the left-hand side, $\log(H_{IF}^2)$ is also plotted as a function of the same variable. Assuming $H_{IF} \propto e^{-\beta n_b}$, we calculated $\beta_{calc} = 2.8$ per C−C bond as compared with the experimental value $\beta_{exp} = 2.6$ per C−C bond. All diabatic couplings were computed at the singlet ground-state geometry with BoysOV localization. The basis is 6-31G**.

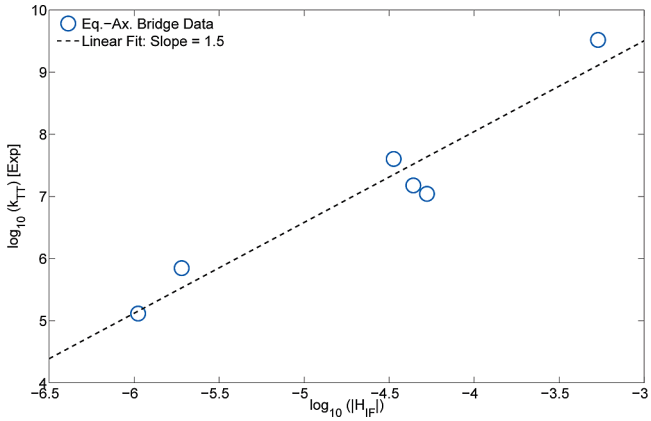

Figure 4. In blue, we plot $\log(|H_{IF}|)$ versus the experimental rate constant $\log(k_{TT}^{exp})$ for triplet−triplet energy transfer when D and A occupy both equatorial and axial positions on cyclohexane. Here, a linear regression plots a line with a slope of 1.5, rather than 2, which could have several explanations. All diabatic couplings were computed at the singlet ground-state geometry with BoysOV localization. The basis is 6-31G**.

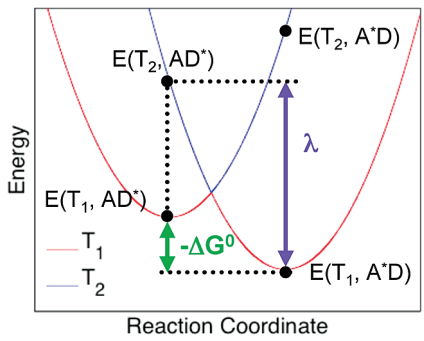

Figure 5. A graphical representation of the free-energy changes (ΔG^0) and reorganization energies (λ) in Table 2.

why our absolute rates are not as accurate as possible for the D-2,6ae and D-2,6ea molecules.

4. Discussion

4.1. Small Mixing Angles and the Condon Principle. The central conclusion of this article is that, together with Marcus theory, the BoysOV and ER localized diabatization algorithms predict EET rates with encouraging success. Admittedly, the near-linear curve in Figure 2 is possible only because the bridge molecules are so rigid that the reorganization energy is effectively constant for the series of molecules considered here. Even with this advantage, however, we were nevertheless surprised that such an excellent correlation between the EET rate and H_{IF}^2 could be achieved using mixing angles as small as those listed in Table 1. In fact, we had expected that, in order to find reasonable diabatic couplings, we would need to find the region of the avoided crossing where mixing angles are necessarily large.

As Figure 2 shows, however, meaningful relative diabatic couplings can be found for the molecules in this paper using only the singlet ground-state geometry, for which the excitation energy of the first excited state T_1 is almost entirely confined to the acceptor and the excitation energy of the second excited state T_2 is almost entirely confined to the donor. Thus, whereas mixing angles under 1×10^{-3} might usually be ignored computationally, our research suggests that even these small diabatic couplings can be quite meaningful for EET rates.

In the future, it will be crucial to investigate why and where the Condon approximation fails[33–36] for a broad series of donors, bridges, and acceptors, so that we may gain experience for choosing the optimal geometry for H_{IF}. In particular, when, if ever, must we optimize the transition-state geometry and search for the avoided crossing? We will surely save a great deal of computational effort if we can safely use the ground-state geometry exclusively for H_{IF} calculations of EET.

4.2. Failure of the Condon Principle for a Flexible Bridge. One case where we have already demonstrated a failure of the Condon approximation is for a flexible CH_2 bridge. In this case, for changes in molecular geometry corresponding to electronic relaxation, we found that the H_{IF} value changed by a factor of more than 10 for compound M in Table 1. This failure of the Condon approximation presents a serious obstacle to using standard Marcus theory in order to predict experimental EET rates. For this reason, we now want to analyze why the Condon approximation fails badly in this case, so that we may better anticipate when standard Marcus theory may be applied.

TABLE 2: Reorganization Energies [$\lambda = E(T_2, AD^*) - E(T_1, A^*D)$] and Energy Shifts [$\Delta G^0 = E_F - E_I = E(T_1, A^*D) - E(T_1, AD^*)$] for the Donor−Bridge−Acceptor Molecules Considered in Table 1[a]

molecule	T_1 (A*D geom.) (Hartree)	T_2 (A*D geom.) (Hartree)	T_1 (AD* geom.) (Hartree)	T_2 (AD* geom.) (Hartree)	λ (eV)	ΔG^0 (eV)	prefactor 10^{16}/(eV)^2/s
D-2,6ee	−1113.62150	−1113.56894	−1113.59804	−1113.59130	0.821	−0.638	1.2
D-2,7ee	−1113.62136	−1113.56919	−1113.59831	−1113.59128	0.818	−0.627	1.2
C-1,4ee	−958.63147	−958.57896	−958.60803	−958.60126	0.822	−0.638	1.2
C-1,3ee	−958.63003	−958.58032	−958.60914	−958.60036	0.807	−0.568	0.94
D-2,6ae	−1113.61365	−1113.56403	−1113.59306	−1113.58358	0.818	−0.560	0.84
D-2,6ea	−1113.61568	−1113.56168	−1113.59039	−1113.58258	0.900	−0.688	1.1
D-2,7ae	−1113.61467	−1113.56327	−1113.59265	−1113.58447	0.821	−0.599	1.0
D-2,7ea	−1113.61331	−1113.56405	−1113.59289	−1113.58383	0.802	−0.555	0.90
C-1,4ea	−958.62251	−958.57148	−958.60038	−958.59255	0.815	−0.602	1.1
C-1,3ea	−958.62577	−958.57178	−958.60106	−958.59526	0.830	−0.672	1.4
M	−764.60581	−764.55236	−764.58487	−764.57506	0.836	−0.570	0.80

[a] The column labeled prefactor refers to the value in eq 1 that multiplies $|H_{IF}|^2$; prefactor = $(2\pi/\hbar)[(1/4\pi k_B T\lambda)]^{1/2} e^{-((\lambda+\Delta G^0)^2/4\lambda k_B T)}$. See Figure 5 for a graphical representation of ΔG^0 and λ in terms of the Marcus parabolas.

TABLE 3: Theoretically Predicted Rates versus Experimental Rates[a]

Symbol	Compound	k_{TT}^{ex} [1,2] (1/s)	k_{TT}^{theor} (1/s)
D-2,6ee		3.1×10^6	5.0×10^6
D-2,7ee		9.1×10^7	3.5×10^8
C-1,4ee	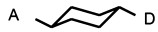	1.3×10^9	3.9×10^9
C-1,3ee		7.7×10^9	2.1×10^{10}
D-2,6ae	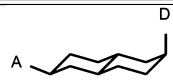	1.3×10^5	1.0×10^4
D-2,6ea		7×10^5	3.9×10^4
D-2,7ae	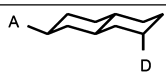	1.1×10^7	2.8×10^7
D-2,7ea	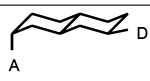	1.5×10^7	1.8×10^7
C-1,4ea	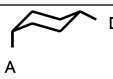	4×10^7	1.3×10^7
C-1,3ea	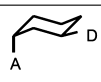	3.3×10^9	3.9×10^9

[a] Here, we use (i) H_{IF} values from the BoysOV function in the ground-state geometry from Table 1 and (ii) the prefactors from Table 2.

In Figures 6 and 7, we overlay the optimized A*D and AD* geometries for the molecules with CH_2 and C-1,4ee bridges. One explanation from these figures is clear to the eye. On the one hand, when the flexible molecule changes from A−CH_2−D* to A*−CH_2−D, a twisting motion occurs, and H_{IF} depends strongly on this relaxation. On the other hand, for a rigid bridge, the geometric relaxation is minimal, and the geometry changes in only very subtle ways; therefore, any changes in H_{IF} should be small. Thus, as we might expect, the Condon approximation is far more unlikely to be obeyed for a flexible bridge as opposed to a rigid bridge.

There is, however, an alternative explanation. There is the possibility that if we interpolate from the initial to final geometry, we will find that both flexible and rigid molecules

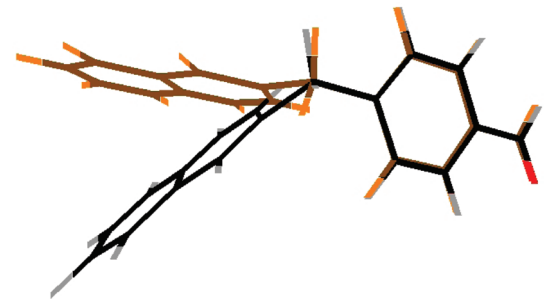

Figure 6. The optimized geometry for the T_1 excited state of the donor−CH_2−acceptor system in the A*D optimized geometry (brown carbon atoms) and the AD* optimized geometry (black carbon atoms).

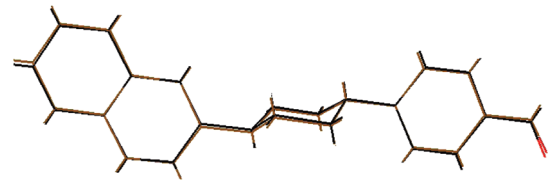

Figure 7. The optimized geometry for the T_1 excited state of the donor−C-1,4ee−acceptor system in the A*D optimized geometry (brown carbon atoms) and the AD* optimized geometry (black carbon atoms).

suffer large changes in $|H_{IF}|$. Moreover, the form of eq 14 suggests that the diabatic coupling H_{IF} might show a peak in the vicinity of the avoided crossing, where the angle θ is presumably maximized. Is it possible that the A*D optimized geometry of the flexible molecule lies close to the avoided crossing and that this explains the apparent failure of the Condon approximation?

In order to refute this explanation, in Figures 8 and 9, we plot the diabatic coupling as we interpolate linearly from the initial to final state for both rigid and flexible molecules. Mathematically, if R_I represents the optimized geometry of AD* and R_F represents the optimized geometry of A*D, we consider the value of H_{IF} along the path

$$R(\zeta) = R_I + \zeta \cdot (R_F - R_I) \tag{15}$$

On the left-hand side of Figures 8 and 9, along this interpolated path in nuclear configuration space, we see an avoided crossing, whereby the first adiabatic excited state switches from D*A to AD* and there is a peak in the mixing

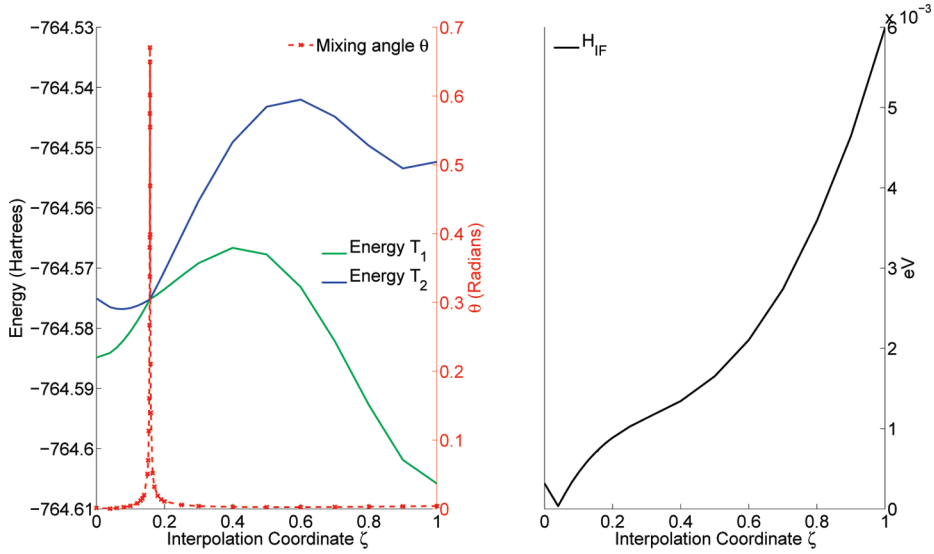

Figure 8. Donor−CH_2−acceptor: On the left-hand side, the energies of the adiabatic first and second excited states are plotted, along with the mixing angle θ along the coordinate ζ in eq 15. $\zeta = 0$ corresponds to AD*, and $\zeta = 1$ corresponds to A*D. On the right-hand side, the corresponding value of H_{IF} is plotted. The dip in H_{IF} at $\zeta = 0.04$ is distinctly to the left of the avoided crossing at $\zeta = 0.16$. The value of H_{IF} grows rapidly far away from the avoided crossing.

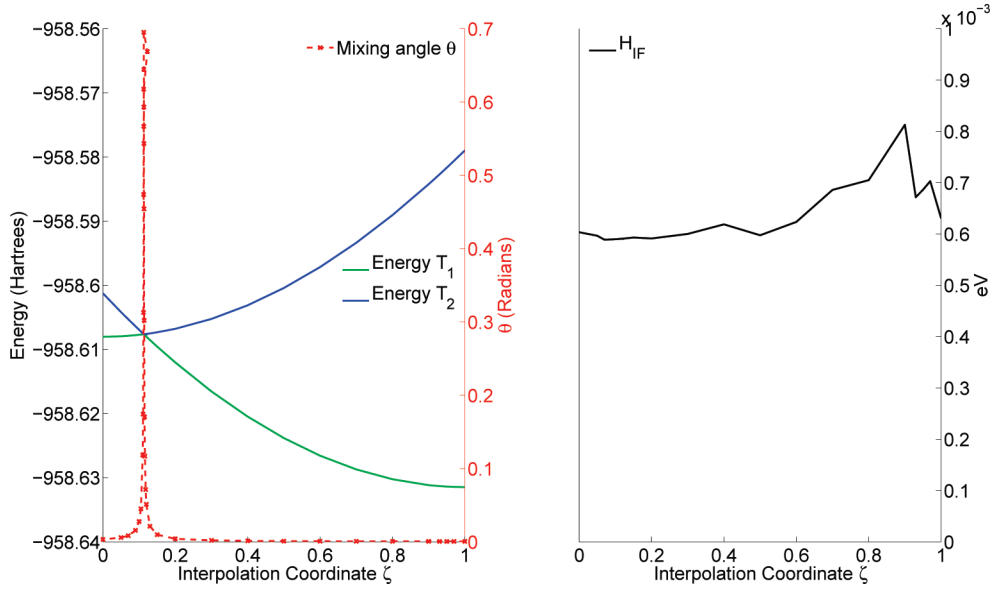

Figure 9. Donor−C-1,4ee−acceptor: On the left-hand side, the energies of the adiabatic first and second excited states are plotted, along with the mixing angle θ along the coordinate ζ in eq 15. $\zeta = 0$ corresponds to AD*, and $\zeta = 1$ corresponds to A*D. On the right-hand side, the corresponding value of H_{IF} is plotted.

angle θ. In Figures 10 and 11, we show attachment/detachment plots[37] for the first two excited triplet states when the flexible molecule sits nearly at the avoided crossing, both before and after we apply our localized diabatization algorithm. At this avoided crossing geometry, the two adiabatic states have delocalized attachment/detachment density, and the mixing angle is $\pi/4$. After localized diabatization, the attachment/detachment densities are localized on either the donor or the acceptor molecule.

On the right-hand side of Figures 8 and 9, we plot the corresponding values of the diabatic couplings $|H_{IF}|$ along the same interpolation path. We conclude that the failure of the Condon approximation for the flexible bridge has very little to do with the avoided crossing. On the contrary, the diabatic coupling is nearly constant in both cases near the avoided crossing, which mirrors previous results in electron transfer.[38] From the graphs, we find that the diabatic coupling grows for the flexible bridge as the energy

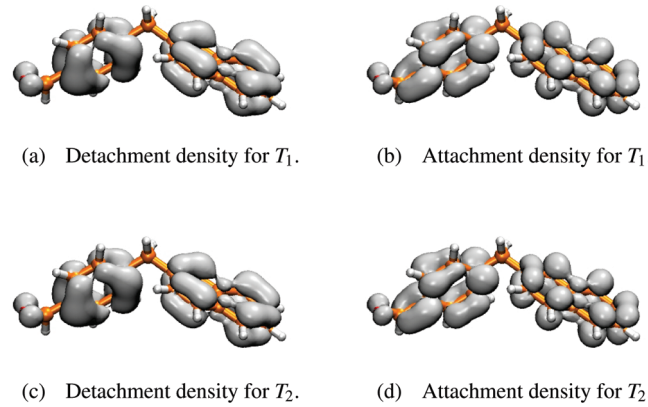

(a) Detachment density for T_1. (b) Attachment density for T_1.

(c) Detachment density for T_2. (d) Attachment density for T_2.

Figure 10. Attachment/detachment plots for the adiabatic excited triplet states near the avoided crossing; see section 4.2. The molecule here is donor−CH_2−acceptor.

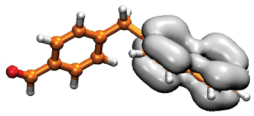

(a) Detachment density for the first localized diabat.

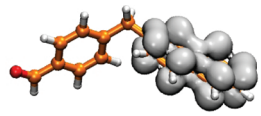

(b) Attachment density for the first localized diabat.

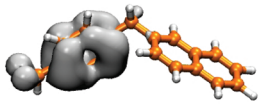

(c) Detachment density for the second localized diabat.

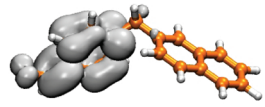

(d) Attachment density for the second localized diabat.

Figure 11. Attachment/detachment plots for the occupied−virtual separated Boys localized diabatic excited triplet states near the avoided crossing; see section 4.2. The molecule here is donor−CH_2−acceptor.

of the adiabatic T_1 and T_2 states grows, and the molecule is exploring a twisting motion.

Overall, these examples suggest that for donor−bridge−acceptor systems with rigid bridges, as opposed to flexible bridges, the Condon approximation for EET is a realistic approximation. For a flexible bridge, a more elaborate theoretical framework is necessary.

5. Conclusions

The results of section 3 show that implementation of either BoysOV or ER localized diabatization gives diabatic coupling elements (H_{IF}) and EET rates that match up well with experiment. For the equatorial−equatorial case in Figure 3, we find $\beta_{calc} = 2.8$ per C−C bond, compared with the experimental value $\beta_{exp} = 2.6$. Because many of the coupling elements in this paper were evaluated at the ground-state geometry of the molecule rather than near the avoided crossing between the two excited states, we may also conclude that, for some cases with rigid bridge molecules, the relative H_{IF} values can be obtained without worrying too much about the exact geometry of the molecule. Future research will benefit greatly from exploring the geometric dependence of $H_{IF}(R)$ in more detail for a broad series of EET or ET reactions. Because the BoysOV and ER algorithms are computationally inexpensive and can be implemented in a black box format, we believe that they will be very useful tools for future computational studies of nonequilibrium transfer reactions.

Acknowledgment. We thank Abraham Nitzan, Yihan Shao, Todd Martinez, Gemma Solomon, David Chandler, Seogjoo Jang, Robert J. Cave, and Marshall Newton for very illuminating conversations. M.A.R. thanks the chemistry division of both the NSF and the ONR for financial support. This work was supported in part by the ANSER Center, an Energy Frontier Research Center funded by the US Department of Energy, Office of Science, Office of Basic Energy Sciences, under Award Number DE-SC0001059.

Appendix

Most of the computational details necessary for implementing ER localization for CIS states have been published previously.[5] For completeness, we now add a few more details regarding how occupied−virtual separated Boys and ER localization routines were implemented for the calculations presented above. We use the notation from section 2.2. For this appendix, many-electron states are indexed with capital letters $\{I, J, K, L, M\}$ and molecular spin orbitals are indexed by lower-case letters; $\{i, j\}$ identify occupied orbitals, $\{a, b\}$ identify virtual orbitals, and $\{p, q, r, s\}$ identify either occupied or virtual orbitals.

1. Occupied-Virtual Separated Boys Localized Diabatization. For standard Boys localization, we maximize the sum

$$f_{\text{Boys}}(\mathbf{U}) = f_{\text{Boys}}(\{\Xi_I\}) = \sum_{I,J=1}^{N_{\text{states}}} |\langle \Xi_I|\vec{\mu}|\Xi_I\rangle - \langle \Xi_J|\vec{\mu}|\Xi_J\rangle|^2 \tag{16}$$

The usual approach for optimizing the function above is to use the method of Jacobi sweeps.[25] For this approach, the only necessary input is the expectation value of the dipole operators in the basis of adiabatic states, e.g., in the x direction, $\langle \Phi_I|X|\Phi_J\rangle$. From these dipole matrices, one may compute the expectation value in any diabatic basis

$$\begin{aligned} |\Xi_I\rangle &= \sum_{J=1}^{N_{\text{states}}} |\Phi_J\rangle U_{JI} \\ \langle \Xi_I|X|\Xi_J\rangle &= \sum_{KL} U_{KI}\langle \Phi_K|X|\Phi_L\rangle U_{LJ} \end{aligned} \tag{17}$$

More concretely, let us assume that we have performed a restricted, closed-shell HF calculation. Singlet CIS states are of the form

$$|\Phi_J^{\text{sing}}\rangle = \sum_{ia} t_i^{Ja}(c_a^\dagger c_i + c_{\bar{a}}^\dagger c_{\bar{i}})|\Phi_{\text{HF}}\rangle \tag{18}$$

and triplet CIS states are of the form

$$|\Phi_J^{\text{trip}}\rangle = \sum_{ia} t_i^{Ja}(c_a^\dagger c_i - c_{\bar{a}}^\dagger c_{\bar{i}})|\Phi_{\text{HF}}\rangle \tag{19}$$

For either case, the corresponding dipole matrices of the adiabatic states are

$$\langle \Phi_I|X|\Phi_J\rangle = 2\left(\sum_i \delta_{IJ}X_{ii} - \sum_{aij} t_i^{Ia}t_j^{Ja}X_{ij} + \sum_{iba} t_i^{Ia}t_i^{Jb}X_{ab}\right) \tag{20}$$

For occupied−virtual separated Boys localization, we split apart the dipole matrices into occupied and virtual components, i.e., $X = X^{\text{occ}} + X^{\text{virt}}$. This decomposition can be justified by expressing X in second-quantized form as $X = \sum_{rs} X_{rs}c_r^\dagger c_s$ and then using the fact that the one-electron density matrix for CIS states is block diagonal; see eq 27. The result is

$$\langle \Phi_I|X^{\text{occ}}|\Phi_J\rangle = 2\left(\delta_{IJ}\sum_i X_{ii} - \sum_{aij} t_i^{Ia}t_j^{Ja}X_{ij}\right) \tag{21}$$

$$\langle \Phi_I|X^{\text{virt}}|\Phi_J\rangle = 2\left(\sum_{iba} t_i^{Ia}t_i^{Jb}X_{ab}\right) \tag{22}$$

and we maximize the localization of each component

$$f_{\mathrm{BoysOV}}(\mathbf{U}) = f_{\mathrm{BoysOV}}(\{\Xi_I\}) = \sum_{I,J=1}^{N_{\mathrm{states}}} |\langle\Xi_I|\vec{\mu}^{\mathrm{occ}}|\Xi_I\rangle - \langle\Xi_J|\vec{\mu}^{\mathrm{occ}}|\Xi_J\rangle|^2 + |\langle\Xi_I|\vec{\mu}^{\mathrm{virt}}|\Xi_I\rangle - \langle\Xi_J|\vec{\mu}^{\mathrm{virt}}|\Xi_J\rangle|^2 \quad (23)$$

Effectively, maximizing eq 23 moves apart the centers of "particle" or virtual excitations and also the centers of the "hole" or occupied de-excitations of the CIS states. We note that this algorithm was suggested to us recently by Klaus Ruedenberg. In general, we much prefer the ER method to this BoysOV approach because (i) the physical meaning of the BoysOV diabatic states is not clear, (ii) ER works both for ET and EET while BoysOV works for only for EET and Boys works only for ET, and (iii) BoysOV diabatic states are defined only for CIS excited states and are not easily extended to other prototypical excited states.

2. Computational Implementation of ER Localized Diabatization. A complete algorithm for applying ER localized diabatization to CIS adiabatic states has already been published.[5] As described previously, in order to implement ER for large systems, the bottleneck is computing the self-interaction four-tensor in the basis of adiabatic states

$$R_{JKLM} = \sum_{I=1}^{N_{\mathrm{states}}} \int \mathrm{d}\underline{\mathbf{r}}_1 \int \mathrm{d}\underline{\mathbf{r}}_2 \frac{\langle\Phi_J|\hat{\rho}(\underline{\mathbf{r}}_2)|\Phi_K\rangle\langle\Xi_L|\hat{\rho}(\underline{\mathbf{r}}_1)|\Xi_M\rangle}{|\underline{\mathbf{r}}_1 - \underline{\mathbf{r}}_2|} \quad (24)$$

$$= \sum_{rspq} D_{rs}^{JK}(rs|pq)D_{pq}^{LM} \quad (25)$$

where $(rs|pq)$ is the two-electron Coulomb matrix element in chemists' notation and the density matrix D is

$$D_{rs}^{JK} = \langle\Phi_J|c_r^\dagger, c_s|\Phi_K\rangle \quad (26)$$

$$= \begin{cases} \sum_i t_i^{Jr} t_i^{Ks} & r,s = \text{virtual} \\ -\sum_a t_r^{Ja} t_s^{Ka} + \delta_{rs}\delta_{JK} & r,s = \text{occupied} \end{cases} \quad (27)$$

Here $c_r^\dagger$ and c_s are creation and annihilation operators for orbitals r and s. We compute the Coulomb integral in eq 25 using the resolution of the identity (RI) approximation,[39] with error measured in the Coulomb metric for variational stability[40]

$$(rs| \approx \sum_{XY} (rs|Y)(Y|X)^{-1}(X| = \sum_X C_{rs}^X (X| \quad (28)$$

and

$$(rs|pq) \approx \sum_{XY} C_{rs}^X (X|Y) C_{pq}^Y \quad (29)$$

Here X and Y are auxiliary basis fitting functions, in this implementation chosen to be the high-quality fitting sets provided by Ahlrichs and co-workers.[41] The fitting basis functions are of the same form as the atomic orbital basis set. (Note the change in capitalized notation here only.)

In general, a minor simplification to eq 29 can be made by computing

$$B_{rs}^X = \sum_Y C_{rs}^Y (Y|X)^{1/2} \quad (30)$$

so that

$$(rs|pq) \approx \sum_X B_{rs}^X B_{pq}^X \quad (31)$$

In our implementation, we perform the contraction over the density matrix before the fitting step

$$\tilde{R}_X^{JK} = \sum_{pq} D_{pq}^{JK}(pq|X) \quad (32)$$

$$\tilde{B}_Y^{JK} = \sum_X \tilde{R}_X^{JK}(X|Y)^{-1/2} \quad (33)$$

to set up the final contraction step

$$R_{JKLM} \approx \sum_Y \tilde{B}_Y^{JK} \tilde{B}_Y^{LM} \quad (34)$$

As there will be few many-electron states $\{J, K, L, ...\}$, the most time-consuming steps are the computation of the molecular orbital basis set integrals $(pq|K)$ (scaling to the fourth power of basis set size). Potentially, converting the density matrix D_{rs}^{JK} into the atomic orbital basis representation could provide additional performance improvement.

References and Notes

(1) Closs, G. L.; Piotrowiak, P.; MacInnis, J. M.; Fleming, G. R. *J. Am. Chem. Soc.* **1988**, *110*, 2652.
(2) Closs, G. L.; Johnson, M.; Miller, J. R.; Piotrowiak, P. *J. Am. Chem. Soc.* **1989**, *111*, 3751.
(3) Marcus, R. A. *J. Phys. Chem.* **1963**, *67*, 853.
(4) Marcus, R. A.; Sutin, N. *Biochim. Biophys. Acta* **1985**, *811*, 265.
(5) Subotnik, J. E.; Cave, R. J.; Steele, R. P.; Shenvi, N. *J. Chem. Phys.* **2009**, *130*, 234102.
(6) Braga, M.; Larsson, S. *J. Phys. Chem.* **1993**, *97*, 8929.
(7) Koga, N.; Sameshima, K.; Morokuma, K. *J. Phys. Chem.* **1993**, *97*, 13117.
(8) Nitzan, A. *Chemical Dyanmics in Condensed Phases*; Oxford University Press: New York, 2006.
(9) Schatz, G.; Ratner, M. A. *Quantum Mechanics in Chemistry*; Dover Publications: Mineola, NY, 2002.
(10) Dexter, D. L. *J. Chem. Phys.* **1953**, *21*, 836.
(11) Jang, S.; Jung, Y.; Silbey, R. *J. Chem. Phys.* **2002**, *275*, 319.
(12) Beljonne, D.; Curutchet, C.; Scholes, G. D.; Silbey, R. J. *J. Phys. Chem. B* **2009**, *113*, 6583.
(13) Jortner, J. *J. Chem. Phys.* **1976**, *64*, 4860.
(14) Barbara, P. F.; Meyer, T. J.; Ratner, M. A. *J. Phys. Chem.* **1996**, *100*, 13148.
(15) Subotnik, J. E.; Yeganeh, S.; Cave, R. J.; Ratner, M. A. *J. Chem. Phys.* **2008**, *129*, 244101.
(16) Farazdel, A.; Dupuis, M. *J. Comput. Chem.* **1991**, *12*, 276.
(17) Rosso, K. M.; Dupuis, M. *Theor. Chem. Acc.* **2006**, *116*, 124.
(18) Sanz, J. F.; Malrieu, J. P. *J. Phys. Chem.* **1993**, *97*, 99.
(19) Cave, R. J.; Newton, M. D. *Chem. Phys. Lett.* **1996**, *249*, 15.
(20) Cave, R. J.; Newton, M. D. *J. Chem. Phys.* **1997**, *106*, 9213.
(21) Voityuk, A. A.; Rosch, N. *J. Chem. Phys.* **2002**, *117*, 5607.
(22) Hsu, C. P.; You, Z. Q.; Chen, H. C. *J. Phys. Chem. C* **2008**, *112*, 1204.
(23) Chen, H. C.; You, Z. Q.; Hsu, C. P. *J. Chem. Phys.* **2008**, *129*, 084708.
(24) Hsu, C. P. *Acc. Chem. Res.* **2009**, *42*, 509.
(25) Edmiston, C.; Ruedenberg, K. *Rev. Mod. Phys.* **1963**, *35*, 457.

(26) Boys, S. F. *Rev. Mod. Phys.* **1960**, *32*, 296.
(27) Foster, J. M.; Boys, S. F. *Rev. Mod. Phys.* **1960**, *32*, 300.
(28) Boys, S. F. In *Quantum Theory of Atoms, Molecules and the Solid State*; Lowdin, P., Ed.; Academic Press: New York, 1966; p 253.
(29) Pipek, J.; Mezey, P. G. *J. Chem. Phys.* **1989**, *90*, 4916.
(30) Kleier, D. A.; Halgren, T. A.; Hall, J. H.; Lipscomb, W. N. *J. Chem. Phys.* **1974**, *61*, 3905.
(31) Subotnik, J. E.; Shao, Y.; Liang, W.; Head-Gordon, M. *J. Chem. Phys.* **2004**, *121*, 9220.
(32) Shao, Y.; et al. *Phys. Chem. Chem. Phys.* **2006**, *8*, 3172.
(33) Troisi, A.; Nitzan, A.; Ratner, M. A. *J. Chem. Phys.* **2003**, *119*, 5782.
(34) Toutounji, M. M.; Ratner, M. A. *J. Phys. Chem. A* **2000**, *104*, 8566.
(35) Medvedev, E. S.; Stuchebrukhov, A. A. *Chem. Phys.* **2004**, *296*, 181.
(36) Troisi, A.; Orlandi, G. *J. Phys. Chem. B* **2002**, *106*, 2093.
(37) Head-Gordon, M.; Grana, A. M.; Maurice, D.; White, C. A. *J. Phys. Chem.* **1995**, *99*, 14261.
(38) Werner, H. J.; Meyer, W. *J. Chem. Phys.* **1981**, *74*, 5802.
(39) Vahtras, O.; Almlø¨f, J.; Feyereisen, M. W. *Chem. Phys. Lett.* **1993**, *213*, 514–518.
(40) Dunlap, B. *THEOCHEM* **2000**, *501*−*502*, 221–228.
(41) Weigend, F.; Häser, M.; Patzelt, H.; Ahlrichs, R. *Chem. Phys. Lett.* **1998**, *294*, 143–152.

JP101235A